Dehydration experiments on natural omphacites: qualitative and quantitative characterization by various spectroscopic methods

M. Koch-Müller[1], I. Abs-Wurmbach[2], D. Rhede[1], V. Kahlenberg[3], S. Matsyuk[4]

[1] GeoForschungsZentrum Potsdam, Department 4, Telegrafenberg, 14473 Potsdam, Germany

mkoch@gfz-potsdam.de

[2] Institute of Applied Geoscience, Technical University Berlin, 10623 Berlin, Germany

[3] Institute of Mineralogy and Petrography, University of Innsbruck, 6020 Innsbruck, Austria

[4] Institute of Geochemistry and Ore Formation, Ukrainian Academy of Science, Kiev-22 142, Ukraine

for **Physics and Chemistry of Minerals**

Key words: natural omphacite, OH incorporation, dehydration, infrared spectroscopy, X-ray structure refinement, Mössbauer spectroscopy, UV/VIS spectroscopy, secondary ion mass spectrometry, IR absorption coefficient for water

Corresponding author:
Monika Koch-Müller
GeoForschungsZentrum Potsdam
Chemie der Erde
Telegrafenberg
14473 Potsdam
Germany

Phone + 49 (331) 288-1492
Fax + 49 (331) 288-1402

mkoch@gfz-potsdam.de

Abstract

A series of natural omphacites from a wide range of P, T occurrences were investigated by electron microprobe (EMP), infrared (IR)-, Mössbauer (MS)- and optical spectroscopy in the UV/VIS spectral range (UV/VIS), secondary ion mass spectrometry (SIMS) and single crystal structure refinement by X-ray diffraction (XRD) to study the influence of hydrogen loss on valence state and site occupancies of iron. In accordance with literature data we found Fe^{2+} at M1 as well as at M2, and in a first approach assigned Fe^{3+} to M1, as indicated by MS and XRD results. Hydrogen content of three of our omphacite samples were measured by SIMS. In combination with infrared spectroscopy we determined an absorption coefficient: $\varepsilon_{i,tot} = 65000 \pm 3000$ $lmol_{H2O}^{-1}cm^{-2}$. Using this new $\varepsilon_{i,tot}$ value, we obtained water concentrations ranging from 60 to 700 ppm H_2O (by weight). Hydrogen loss was simulated by stepwise heating the most water rich samples in air up to 800 °C. After heat treatment the samples were analyzed again by IR, MS, UV/VIS and XRD. Depending on the type of the OH defect, the grade of dehydration with increasing temperature is significantly different. In samples relatively poor in Fe^{3+} (< 0.1 Fe^{3+} pfu), hydrogen associated with vacancies at M2 (OH bands around 3450 cm^{-1}) starts to leave the structure at about 550 °C and is completely gone at 780 °C. Hydrogen associated with Al^{3+} at the tetrahedral site (OH bands around 3525 cm^{-1}, Koch-Müller et al., 2004*)* remains completely unaffected by heat treatment up to 700 °C. But all hydrogen vanished at about 775 °C. However, this is different for a more Fe^{3+}-rich sample (0.2 Fe^{3+} pfu). Its IR spectrum is characterized by a very intense OH band at 3515 cm^{-1} plus shoulder at 3450 cm^{-1}. We assign this intense high energy band to vibrations of an OH dipole associated with Fe^{3+} at M1 and a vacancy either at M1 or M2. OH release during heating is positively correlated with decrease in Fe^{2+} and combined with increase in Fe^{3+}. That dehydration is correlated with oxidation of Fe^{2+} is indirectly confirmed by annealing of one sample in a gas mixing furnace at 700 °C under reducing conditions

keeping almost constant OH^- content and giving no indication of Fe^{2+}-oxidation. Obtained data indicate that in samples with a relatively high concentration of Fe^{2+} at M2 and low water concentrations, i.e. at a ratio of $Fe^{2+M2}/H > 10$ dehydration occurs by iron oxidation of Fe^{2+} exclusively at the M2 site following the reaction: $[Fe^{2+[M2]} \cdot OH^-] = [Fe^{3+[M2]} \cdot O^{2-}] + 1/2\ H_2\uparrow$. In samples having relatively low concentration of Fe^{2+} at M2 but high water concentrations, i.e. ratio of $Fe^{2+M2}/H < 5.0$ dehydration occurs through oxidation of Fe^{2+} at M1.

Introduction

Clinopyroxene (cpx) is a major constituent of the Earth's crust and mantle. From experimental studies as well as from studies of natural systems it is well known that cpx can store hydrogen in its structure with concentrations ranging from 30 to 3000 ppm H_2O (by weight). The highest concentrations are found in clinopyroxenes that come from ultrahigh pressure metamorphic terrane (e.g. Katayama et al., 2006). But some of our high pressure candidates (e.g. TM-8, estimated P: 4.4 GPa; A-45/2, estimated P: 5.5 GPa; DB22, estimated P: 4.0 – 4.5 GPa) show concentrations as low as 30-50 ppm H_2O (Koch-Müller et al. 2004). Such low water concentration can be explained e. g. by (i) low water activity in the high pressure rocks or (ii) hydrogen loss during uplift of the minerals to the surface. For Fe-bearing minerals the reaction which is generally assumed to control the hydration-dehydration involves reduction-oxidation of iron: $[Fe^{2+} \cdot OH^-] = [Fe^{3+} \cdot O^{2-}] + 1/2\ H_2\uparrow$. Ingrin and Skogby (2000) estimate on the basis of Fe^{3+} concentrations of mantel cpx a maximum water loss of 450 – 900 wt ppm.

The main focus of this study is to see whether or not low water concentration in omphacites can be explained by dehydration processes during uplift. We investigated omphacites from different occurrences concerning localities and depths using infrared, Mössbauer- and optical spectroscopy

as well as single crystal X-ray diffractions. And additionally we simulated hydrogen loss through heating the same crystal in air and stepwise analysing the samples by the above mentioned methods. From our experiments it seems to be evident that dehydration of omphacite is coupled with oxidation of iron and that this takes place in a very fast process.

Sample selection and sample treatment

We selected eight omphacites and one omphacitic pyroxene (< 5 mole% jadeite component) from different geological settings (Table 1). Four samples originate from eclogites of kimberlite pipes in South Africa and Yakutia (Siberia) and experienced relatively high pressures and temperatures (DB-22, SA, Tw-297/77 and Sl-415). The omphacitic sample TW-2 was also collected at a kimberlite pipe but in this case from a granulite of low P and relatively high temperature origin (Table 1). Three samples are from eclogites of the Münchberger massive being exposed to from relatively low P and T regimes (1131, FTS-9 and SB01-6). The ninth sample (Ur-1) from eclogite of the Maksyutowskiy complex, South Ural in Russia, experienced low pressure and very low temperature. Samples were chosen with Na content ranging from 0.1 – 0.4 pfu and with varying iron contents.

The selected crystals are green to gray in colour and several hundred micrometer in diameter. At the first view the single crystals are optically clear but careful optical microscopy showed in some parts of the crystals the presence of solid inclusions from µm to nm. Inclusion-rich parts are located at the rim of the crystals and/or along cleavage planes and/or they form veins within the optically clear parts. One sample (TW-297) was investigated by transmission electron microcopy (Koch-Müller et al., 2004) and the inclusions were identified as nm-sized sheet silicates of clinochlore composition with minor impurities of iron (< 2 mol % Fe^{2+} pfu). Optical clear cpx without cracks were hand picked from the host

xenoliths. We assume, that the small amount of Fe in the clinochlore inclusions, if present, will not contribute significantly to the absorption in our Mössbauer spectra.

Prior to heat treatment all samples were analyzed by Electron microprobe, Mössbauer and NIR spectroscopy. Additionally, some samples were investigated by spectroscopy in the UV/VIS and by single crystal X-ray diffraction.

To probe the dehydration mechanism we annealed the samples in air using a Heraeus K1256 furnace. After reaching the desired temperature all samples were placed at the same spot within the furnace. Temperature uncertainty is estimated as ± 2%. Polished crystals of samples SA, Sl-415, Ur-1, TW-2 were stepwise heated in air up to 775 °C. We started the annealing at 550 °C and increased the temperature in 25 - 50°C steps. At each temperature step the sample was hold for 24 hours then quenched and investigated by FTIR spectroscopy and optical spectroscopy (UV/VIS). For Mössbauer spectroscopy about 9 – 80 mg of the material was crashed and ground to a fine powder prior to annealing in air for 3-4 hours. One crystal of sample SA was annealed for 24 hours under controlled oxygen fugacity of $10^{-18.5}$ bar at 800 °C (close to the magnetite/wüstite buffer) in a vertical rapid-quench furnace. The oxygen fugacity was controlled by a mixture of CO_2 and H_2 gas that flowed past the specimen. Oxygen fugacity was monitored using a zirconia-based solid electrolyte oxide sensor with air as reference gas.

Analytical Techniques

Electron microprobe (EMP) analyses of all nine samples were performed with a Cameca SX50 and SX100 microprobes at the GeoForschungsZentrum Potsdam using the wavelength dispersive mode. The operating conditions were 15 kV and 20 nA. Counting time was set at 20 s on peak and 10 s on background. Well characterized natural minerals were used as standards: diopside (Si, Ca), K-feldspar (Al, K), olivine

(Mg), albite (Na), hematite (Fe), rhodonite (Mn), rutile (Ti) and chromite (Cr). Raw spectrometer data were corrected with the PAP program (Pouchou & Pichoir, 1985). One sample was analyzed after the heat treatment to insure that composition of the crystals does not change during the annealing.

Mössbauer spectroscopy

^{57}Fe Mössbauer spectra were obtained at the TU-Berlin using a 1.85 GBq ^{57}Co in Rh source. Spectra were taken at RT with a 1024 multichannel analyzer using a constant electrochemical drive system with symmetric triangular velocity wave form (Halder Electronic, Germany). Normally, runs were performed in the velocity range of +/- 4 mm/s, and additionally some at +/- 10 mm/s to check for magnetically ordered iron phases. Velocity scale and isomer shift was calibrated against natural iron (α Fe-foil, 25 mm thickness 99.99% purity). IS-shifts from calibration spectra were used as gravity centre for the fitting procedure.

Omphacite powder samples were diluted under adding 60 to 100 mg sugar followed by homogenization and, under avoiding intensive pressure filled in alumina rings (diameter 10 mm, height 1.5 mm). Thus we succeeded in getting spectra free of texture effects, as indicated by allowing unproblematic immediate fitting with doublets (c.f. Koch-Müller et al., 1999). Accumulated counts per channel were about 10^6. Using the modified program "MBF" (Nagel, 1990) the simultaneously obtained two spectra (512chanels each) were folded and evaluated assuming Lorentzian line shape (Abs-Wurmbach & Amthauer, 1988). We tried to keep, if possible, all variables free, i.e. without applying constrains. Convergence was reached in all cases but one (Ur-1). Here it was only possible to gather very small quantity of natural omphacite (less than 2 mg $Fe°_{tot,}$) thus resulting in linear absorbance intensities (T% of single doublet lines of Fe^{2+}-sites) with less than 0.2%. This aroused some problems in the fitting procedure,

as here convergence was not reached. Relative errors of area% were calculated on the basis T% and HW(full half width at half height) and their errors, applying the 'potential product law for error progression' (Sachs, 1972).

Spectroscopy in the IR and VIS/UV

For each sample at least two wafers, in (010) and in (100) orientations were prepared. Orientations were determined by optical microscopy under conoscopic observation. Each side of the wafers was polished using a diamond paste (grain size 0.8 micron). Thickness of the grains ranged from 100 to 400 μm and was measured with a digital micrometer.

We collected unpolarized and polarized single-crystal spectra in the IR and visible light using a Bruker ISF 66v spectrometer attached with a Hyperion microscope. IR spectra of all nine samples were scanned in the range of 2500 to 4000 cm^{-1} to detect the OH stretching vibrations using a Globar light source, a KBr beamsplitter and an InSb detector. Some samples were also measured in the range of 8000 – 25000 cm^{-1} using a tungsten light source, a quartz beamsplitter and a Si diode.

Polarized optical spectra were collected with a KRS5-polarizer with the electrical vector of the polarized radiation E parallel to the optical indicatrix axes ($E \parallel n_\gamma$, $E \parallel n_\alpha$ and $E \parallel n_\beta$) . Spectra were taken in optically clear parts of the crystals with an aperture of 80 x 80 μm.

To quantify the hydrogen content we calculated the total absorbances of the OH bands by summing up the integral absorbances along the indicatrix axis $A_{i,\,tot} = A_{n\alpha} + A_{n\beta} + A_{n\gamma}$ and using the calibration obtained in this study (see below).

Polarized single crystal spectra in the range of 30000 to 12000 cm^{-1} were scanned in a single-beam microspectrometer (Zeiss UMSP 80) using UV transparent 10 x objectives (Zeiss ULTRAFLUAR) as condenser and objective. The instrument is operated in a wavenumber step-scan procedure. Details of the measurements are given in Langer (1988).

Secondary Ion mass spectrometry

The hydrogen contents of three omphacite samples were analyzed by Secondary Ion Mass Spectrometry (SIMS) using the CAMECA ims 6f ion probe at the GFZ Potsdam. A 100 nA mass-filtered primary $^{16}O^-$ beam was accelerated to 12.5 kV and focused to form a ~60–80 µm diameter beam at the sample surface. An 8-min pre-sputtering was applied to reduce surface contamination. More technical details are given in Koch-Müller et al. (2006). Prior to each analytical session the entire instrument was baked for at least 48 hours. Counting times per cycle were 10 s for ^1H and 2 s for ^{30}Si. The duration of sputtering required to achieve steady-state conditions (i.e., $^1H^+/^{30}Si^+$ ratio becoming constant) varied as a function of the H_2O concentration and hence the total time of data acquisition often need to be extended to over 120 minutes for the most H depleted samples. For $^1H^+$ measurements relative sensitivity factors were determined from multiple analyses of seven gem quality garnet reference samples whose H_2O content which range between 17 and 870 ppm had been established independently using other techniques (Maldener et al., 2003). The $^1H^+/^{30}Si^+$ ratios used to establish the working curve were calculated by averaging only the final 50 cycles from each analysis. Repeated, independent analytical sessions using a $^{16}O^-$ primary beam demonstrate the critical importance of recalibrating the relative ion yields, as the slope of the calibration line was found to change by as much as 13 % between sessions despite using identical instrument settings and having similar vacuum conditions (Rhede and Wiedenbeck, 2006).

Single crystal X-ray diffraction

Single crystal diffraction data were collected on a Stoe IPDS-2 imaging plate diffractometer using irregular shaped fragments of good optical quality which were mounted on the tip of glass fibers. After data collection the morphology of the samples was approximated by external faces and an analytical absorption correction based on the indexed faces was applied in each case. Further data reduction included Lorentz- and polarization corrections. Based on values on electron occupancy of each site from the site scattering refinements we optimized for the correct site assignment of the multiple substituents in the omphacite samples by using the program OccQP (optimization of site occupances in minerals using quadratic programming).

Results

Characterization of the samples prior to heating

Considering the major elements all but two samples (TW-2 and Ur-1) are very close in composition with a diopside component ranging from about 40 - 60 mole%, a jadeite component of 25 - 35 mole % and a very low hedenbergite component of 3 – 12 mole %. The granulite sample TW-2 has a very low jadeite component of 2 mole% and a diopside component of 71 mole% and is classified as an omphacitic pyroxene. Sample Ur-1 from crustal origin has a significant higher acmite component of 20 % (Table 2) compared to the others cpx which range from 2.5 to 8.5 % at maximum. We included Ur-1 in our study because of its specific composition in respect to iron. Samples which experienced the highest pressure show a higher K concentration than the low-P cpx. For almost all omphacites the jadeite component is high but there is no correlation between the jadeite component and pressure.

Fig. 1 shows polarized IR spectra of selected samples with E ∥ n_γ. Spectra of all samples show two OH stretching bands but with different intensities. In a recent study Koch-Müller et al. (2004) concluded that group-1 bands (around 3450 cm^{-1}) are correlated with cation vacancies at M2 (v^M + 2H) and group-2 bands (around 3530 cm^{-1}) with incorporation of trivalent cations. For example in sample SA the group-2 band is associated with Al at the tetrahedral site and we speculate that for sample Ur-1 the group-2 band is associated with Fe^{3+} at M1 and a vacancy either at M1 or at M2 charge balanced by hydrogen (Fe^{3+M} + v^M + H). This is supported by microprobe analyses as the sum of the jadeite and acmite component of sample Ur-1 exceed the sodium content by 0.03 indicating the presence of excess Fe^{3+}. In a recent study, Stalder and Skogby (2007) could prove by their experiments that in synthetic Fe-bearing opx the latter defect plays an important role in dehydration processes.

Water content of three different samples have been determined by SIMS. In combination with the infrared data we calculate an integrated molar absorption coefficient for water in omphacite of $\varepsilon_{i,tot}$ = 65000 ± 3000 $lmol_{H2O}^{-1}cm^{-2}$ (Table 3). Using this new $\varepsilon_{i,tot}$ value we determined water concentrationsin our omphacites ranging from 60 to 700 ppm H_2O (by weight) (Table 1).

The Fe-content defined as FeO and calculated from electron microprobe analyses range from 4.37 – 11.33 wt %. From Mössbauer spectroscopy we derived Fe valence states and site occupancies. As well known from several studies Fe^{2+} prefers the more distorted M2 site and Fe^{3+} the octahedral M1 site (e. g. Dyar et al., 1989; Oberti and Caporuscio, 1991; Li et al., 2005). According to Rossi et al. (1987) the M2 site may also be occupied by small amounts of Mg. In case of (Fe^{2+} and Mg)-M2 site occupation the M2 site splits into a M2' position approximately 0.4 Å along the b-axis and toward the oxygen atoms O1 and O2, i.e. close to the position and coordination of Fe^{M2} of clinoferrosilite. Although more regular, the new M2' position is still higher distorted than the M1 site (Rossi et al., 1987). Following Dyar et al. (1989) and Li et al. (2005), we

assigned the MS doublet with the highest quadrupole splitting to Fe^{2+} at the more regular M1 site, the doublet with lower quadrupole splitting to Fe^{2+} at the distorted M2 site and the MS doublet with low quadrupole splitting is assigned to Fe^{3+} at M1 (Table 4). Fig. 2 shows a Mössbauer spectrum of sample DB22, which is nearly identical with a cpx spectrum published by Dyar et al. (1989) from San Carlos cpx in comparison to a spectrum of sample Ur-1 with the high acmite component. Table 2 lists the composition results for all samples on the basis of the values obtained by microprobe analysis combined with those of the Mössbauer experiments. Fe^{2+} at M1 range from 0.026 to 0.080 pfu, Fe^{2+} at M2 from 0.043 to 0.186 pfu and Fe^{3+} at M1 from 0.025 to 0.195. Fe^{2+} fractionates into M2, resulting in $Fe^{2+\ M2}/(Fe^{2+\ M1\ and\ M2})$ ratios of 0.518 to 0.699.

The symmetry of the crystal structure of cpx depends on the temperature of crystallization and on composition (Carpenter,1983). In accordance with these observations omphacite, omphacitic cpx grown at high temperatures (Table 1) as well as the cpx with the high acmite component (Ur-1) crystallize in space group C 2/c whereas omphacites grown at low temperature crystallize in space group P 2/n (Table1).

Single crystal X-ray diffraction confirms the presence of Fe^{2+} on both sites: Shown below is (i) the site distribution for cpx DB22 using the combined EMS and Mössbauer spectroscopic results and additionally (ii) the site distribution of the same crystal obtained from single crystal X-ray refinement in combination with optimization of site occupancies using quadratic programming OccQP (Wright et al., 2000) :

(i) $(Na_{0.327}Ca_{0.571}Fe^{2+}_{0.105})^{M2}\,(Mg_{0.521}Al_{0.323}Fe^{2+}_{0.080}Fe^{3+}_{0.035}Ti_{0.045})^{M1}\,(Si_{1.943}Al_{0.057})O_6$

(ii) $(Na_{0.321}Ca_{0.561}Fe^{2+}_{0.072})^{M2}\,(Mg_{0.515}Al_{0.310}Fe^{2+}_{0.100}Fe^{3+}_{0.022}Ti_{0.034})^{M1}\,(Si_{1.968}Al_{0.032})O_6$.

Scattering refinements were used as input for OccQP to obtain (ii) the electron occupancy of sites and by this to be able to find the best-fit between

chemical analysis and X-ray scattering. The results of these two methods are in fair agreement.

Fig. 3 shows the optical spectrum of the most Fe^{3+}-rich sample Ur-1 from 3000 to 30000 cm^{-1}. The peak at 3500 cm^{-1} is due to OH-stretching vibrations. According to Burns (1993) the bands around 10.000 and 8000 cm^{-1} are assigned to crystal field bands (CFB) of Fe^{2+} at M1 which is consistent with small distortion of the octahedral polyhedron. CFB at 9000 and 4500 are assigned to Fe^{2+} at the largely distorted 6 – 8 fold coordinated M2 site (Rossi et al., 1987). The broad and intense feature around 14000 cm^{-1} is induced by Fe^{2+}- Fe^{3+} charge transfer. At 23000 and 27000 cm^{-1} very weak spin forbidden CFB of Fe^{3+} at M1 were observed. Though this sample has about 10 times more Fe^{3+} than the other samples there is no chance to quantify Fe^{3+} concentrations by optical spectroscopy. However, with optical spectroscopy we are able to monitor changes in Fe^{2+} concentrations at M1 and M2 after annealing some samples in air (see below). Optical spectra in the visible strongly differ from sample to sample, reflecting the different concentrations and local arrangements concerning symmetry relations and neighbours (ligands) of Fe (Fig. 4).

Characterization of the samples after heating

Single crystals and powders of four samples (SA, TW-2, Ur-1, Sl-415) were annealed in air for 24 h (crystals) and 6 h (powders) and investigated with the above mentioned methods, i.e. the powders were used for Mössbauer Spectroscopy and the single crystals for optical and infrared spectroscopy as well as for X-ray diffraction. The thickness of the 1 to 2 mm sized crystals ranged from 140 – 160 µm. Electron microprobe analyses of one annealed sample (SA) indicated that during annealing only oxidations occurs – no loss of Na was observed. Comparison of infrared spectra of a sample annealed for 24 h under controlled low oxygen fugacity of $10^{-18.5}$ bar and the same sample (with the same thickness and orientation) annealed for 24 h in air indicate that dehydration in omphacite must be associated with oxidation of Fe^{2+} (Fig. 5 a). The grade of

dehydration under heat treatment in air, i.e. under oxidizing conditions is more than ten times higher than for the same crystal annealed at the same temperature but under reducing conditions of $10^{-18.5}$ bar. However, as observed by Blanchard and Ingrin (2004) kinetic of hydrogen diffusion is much slower under reducing conditions and to exclude that the reason for our observation is only a slower kinetic under reducing conditions we measured OH concentration profiles from core to rim of the mm sized crystals with a spatial resolution of 80 µm. As the remaining hydrogen content in all the heat treated samples (also those discussed below) was homogenous distributed from core to rim we believe that we reached for each specific temperature in 24 h an equilibrium concentration. If the difference in the H concentration of the above mentioned samples were only a matter of kinetic we should observe a concentration profile with un- or less depleted regions in the core and increasing depletion to the rim (e.g. Woods et al., 2000), which was not the case.

Fig. 6a and 6b show some selected IR spectra, i.e. sample SA and Ur-1, respectively, before and after heat treatment at increasing temperatures performed under oxidizing conditions (air). At each temperature the samples were hold for 24 hour in air and quenched to investigate them by spectroscopy. IR spectra taken at different spots on the crystals revealed that the remaining OH concentration for each temperature was homogenous distributed over the crystall indicating again that we reached an equilibrium concentration for that specific temperature (see above). The two groups of OH bands of the two samples behave different: in sample SA hydrogen associated with vacancies at M2 (group-1 bands) starts to leave the structure at about 550 °C. Hydrogen concentrations associated with Al^{3+} at the tetrahedral site (group-2 bands) remain constant up to 700 °C. But all hydrogen is gone at 780 °C. Group-1 OH bands of sample Ur-1 with the high acmite component and excess Fe^{3+} react in the same way with increasing temperatures as sample SA does but the group-2 OH bands behave different. For these bands the grade of dehydration with increasing

temperature is the same as for the group-1 bands. We assume that in Ur-1 incorporation of group-1-hydrogen is associate with Fe^{3+} at M1 plus a vacancy most probably at M1 ($Fe^{3+M} + v^{M} + H$) and dehydration could therefore partly be accompaigned by reduction of already incorporated Fe^{3+} (Stalder and Skogby, 2007). Both types of defects of sample Ur-1 are related to vacancies and may explain why both defects behave similar during the dehydration and different to the Al-based defects of sample SA. For comparison: Generally, dehydration of the cpx is at all quite different to dehydration of olivine. In IR spectra of an olivine sample containing about 400 wt ppm water Koch-Müller et al. (2006) observed nearly no change in OH concentration after heat treatment (750 °C for 24 hours in air) although the crystal has about the same size and shape as our cpx crystal. This indicates that the large M2 sites in cpx may play an important role in the velocity of their dehydration process.

Fig. 7 and 8 compares Mössbauer spectra of samples taken before and after annealing. Their Mössbauer parameters are given in Table 5. Sample TW-2 (Fig. 7) was tempered at 800 °C. Fe^{3+} concentration increases during heat treatment whereas Fe^{2+} at M2 significantly decreases. Site occupancy of Fe^{2+} at M1 of the untreated sample almost coincide within limits of errors (2s) with the annealed 800 °C sample, but significantly decreases on M2, i.e. oxidation occurs at the M2 site (see discussion). Therefore, expecting a second Fe^{3+} - doublet at M2, we performed also a Mössbauer fit with 4 doublets (4D fit) – two doublets for Fe^{2+} at M1 and M2 and two for Fe^{3+}. Since lines of Fe^{3+} doublets at low intensities have a tendency to smear to not separated lines, we applied some fixed parameters (see Fig. 7 and Table 5). The resulting sum of Fe^{2+} and Fe^{3+} site occupancies at (M1+M2) obtained by the 4D fit is in accordance with that of the 3D fit. Furthermore, Fe^{2+} at M1 is within limits of error approximately the same value as obtained for the untreated sample. With heating a significant increase of $Fe^{3+}{}_{tot}$ from 23 to 33 area % in respect to the unheated sample was determined. Concluding from the parameter of the 4D fit this increase seems to be located exclusively at M2. Therefore,

we assume that a 4D fit for the annealed and herewith by dehydration oxidized samples might be also for the other samples a reasonable approximation to Fe^{3+} -site distributions. Obtaining these positive results, we decided to use in the 4D fits for refinement of the two Fe^{2+}-doublets their fixed parameters of the 3D-fit (c.f. Table 5) exclusive the intensity parameter of linear absorption (T%). Fe^{3+} -parameters of both doublets were kept free so far as possible. Sample SA (Fig. 8) was tempered at 775 °C. Here again, site occupancy of Fe^{2+} at M1 (31%) of the untreated sample almost coincide with the 775 °C sample, whereas Fe^{2+} at M2 (53%) significantly decreased for SA775°C (43%) and proportional $Fe^{3+}{}_{tot}$ increased from 16% to 22% heated. These relations are similar to those observed for TW-2. For sample SL-415 4D fits were omitted, since all trials resulted in some physical irrational parameters. In contrast to the two samples mentioned above Mössbauer spectra of the annealed samples at 650 and 750 °C exhibit a small but significantly lower site occupancy of Fe^{2+} at M1 and no change for M2 site compared to the untreated sample (Fig 8). Fe^{3+} is significantly enriched in the heat treated samples and additional Fe^{3+} might preferably occupy the M1 site. Furthermore, site occupancies at 650 and 750 °C are identical within limit of errors. This is also valid for the area sums of the two Fe^{2+} positions. Thus, one may conclude that at 650 °C dehydration processes including oxidation of Fe^{2+} at the M1 site are completed. Pyroxene Ur-1 falls out of the normal composition in this study. It is the richest in acmite component and additionally in hydrogen content (Table 2). Here Fe^{3+} is the dominant species of iron and is further enriched after heating at 700 °C (3D fit, Fig. 8). Different to the SA and TW-2 sample heating leads in both fits (3D and 4D) to a small, but significant decrease of Fe^{2+} in both sites, thus reducing the sum of Fe^{2+} from 30 to 22 area%. Consequently, this is correlated with an increase of Fe^{3+} from 70 (ambient) to 78 area% for both fits. Dehydration of this sample is also controlled by oxidation – but at both sites, M1 and M2 (see discussion). According to their chemistry and their response to annealing we can distinguish two types of omphacites: type A, represented by sample SA and

TW-2 are characterized by high concentration of Fe^{2+} at M2 and relatively low hydrogen content, thus showing a $Fe^{2+\ M2}$/H ratios > than 10 (Table 2). Analysis of the spectra of Fig. 7 and 8 revealed that during heat treatment the Fe^{3+} content increases and Fe^{2+} content at M2 decreases. Fe^{2+} concentration at M1 does not change significantly. Our Mössbauer spectra in combination with the IR spectra (Fig. 5) indicate that during heat treatment dehydration occurs and that the charge is balanced through oxidation of iron at the neighboring M2 site. Thus, we may expect two Fe^{3+} doublets one for Fe^{3+} at M1 and the other for Fe^{3+} at M2.

Type B is represented by sample Sl-415. It is characterized compared to TW-2- and SA-cpx by relatively lower Fe^{2+} concentration at M2, and relatively higher water content, showing a $Fe^{2+\ M2}$/H ratio of 4.1. Analysis of the spectra of sample Sl-415 (Fig. 8) before and after heat treatment reveal that during annealing Fe^{3+} concentration increases but different to samples of type A, Fe^{2+} at M1 decreases while Fe^{2+} at M2 remains more or less constant. Sample Ur-1 represents an intermediate type with Fe^{3+} increase during annealing on both sites. It is also characterized by a low $Fe^{2+\ M2}$/H ratio of 2.0. But it differs from the other samples by its low temperature of formation, its chemistry exhibiting high Fe^{3+}- content (Table 1) and its incorporation mechanism for group-1-hydrogen (associate with Fe^{3+} at M1, see above). Analysis of the MS-spectra of sample Ur-1 before (Fig. 2) and after heat treatment (Fig. 8) confirm the increase of Fe^{3+} during annealing as observed in the other samples but it shows in this case different to Sl-415 a decrease of Fe^{2+} at both sites, M1 and M2 (Table 5).

From our MS-spectra we can exclude - even for the most Fe^{3+}-richest sample - the presence of a Fe^{3+} consuming dehydration mechanism as described by Stalder and Skogby (2007) for Fe-bearing enstatite.

Absorption spectra in the VIS/NIR support these observations. CFB of Fe^{2+} at M1 and M2 strongly overlap in the visible spectral range but due to

strong distortion of the M2 site one low energy transition component of the CFB of Fe^{2+} at M2 can be observed in the NIR (Fig 3) without any band overlap. Fig. 5 and 9 compare CFB and NIR spectra of samples SA, Ur-1 and Sl-415 before and after annealing in air. As expected from Mössbauer spectroscopy, for sample SA the crystal-field-band intensity of Fe^{2+} at M1 remains constant but that of Fe^{2+} at M2 clearly decreases (Fig 5). In contrast to these observations for cpx SA, in sample Sl-415 concentration of Fe^{2+} at M2 remains almost unchanged after annealing (Fig. 9 a). As already mentioned in the presentation of Mössbauer spectroscopic results, sample Ur-1 builds an intermediate type, as here Fe^{2+} intensity of both Fe^{2+} - CFB (Fig. 9 b,c) decrease.

Table 7 summarizes the chemical shifts in H, Fe^{2+} and Fe^{3+} as result of the heat treatment of the four samples named above. In all four samples increase of Fe^{3+} pfu as determined by Mössbauer spectroscopy correlates with decrease of Fe^{2+} and of H pfu. The latter correlation is well pronounced in sample SA and Sl-415 whereas in sample TW-2 the increase of Fe^{3+} and decrease of Fe^{2+} coincides but exceeds the loss of hydrogen. This may be due to the high annealing temperature 800 °C where further annealing of the already dehydrated samples results in increase of Fe^{3+} associated with other defects for charge balancing.

We studied also the influence of annealing on single crystal diffraction data of two samples: DB22 and SA. To do so, crystals were heated on a platinum foil at 800°C for 24h. After quenching in air the crystals were re-mounted on glassfiberand intensities were re-collected. Comparison of the electron occupancy of each site before and after quenching yields no significant difference in the site scattering of both samples. Thus, we cannot observe any significant change in the Fe^{2+} and Fe^{3+} concentration and fractionation due to the annealing. X-ray diffraction seems to be not

sensitive enough to confirm our spectroscopic results.

Discussion

Water quantification

Katayama et al. (2006) investigated natural omphacites from eclogites from the Kokchetav massif by infrared spectroscopy and ion micro-probe measurements. They calculated an averaged absorption coefficient of 83400 ± 14600 $lmol_{H2O}^{-1}cm^{-2}$ from unpolarized infrared spectra using an orientation factor of 1/3. Using unpolarized spectra for quantification introduces high nonsystematic errors especially for minerals with highly anisotropic OH band distribution such as omphacite. The large uncertainty in the absorption coefficient given by Katayama et al. (2006) is reflected in the large standard deviation of the mean value. Individual values range from 70000 to 100000 $lmol_{H2O}^{-1}cm^{-2}$. The absorption value determined in this study of $\varepsilon_{i,tot}$ = 65000 ± 3000 $lmol_{H2O}^{-1}cm^{-2}$ is in good agreement with absorption coefficients of cpx and opx given by Bell et al. (1995), if we take into account the frequency dependence of the absorption coefficient: absorption coefficient trends of OH in hydrous minerals (Paterson, 1982 and Libowitzky and Rossman, 1997) are based on a negative correlation between the IR absorption coefficient for water and the mean wavenumber of the corresponding OH pattern. From this relation we expect for the omphacites investigated by Katayama et al. (2006) a lower value as given by them because the mean wavenumber of band positions of their omphacites is higher than in ours. We believe that due to the unpolarized measurement in the study of Katayama et al. (2006) the OH absorption is overestimated. In addition to this uncertainty it is not quite clear whether

the total absorbance given by Katayama et al. (2006) only reflects intrinsic OH in omphacite. Koch-Müller et al. (2004) showed that the high energy band at 3600 cm^{-1} can also be related to nm sized inclusions of secondary sheet silicates.

Dehydration of cpx

Our data indicate that for cpx with relatively high Fe^{2+} concentration at M2 (around 0.1 pfu) and low water content (< 0.01) dehydration occurs combined with iron oxidation at the M2 site (Tab. 2) following the reaction:

$[Fe^{2+[M2]} \cdot OH^-] = [Fe^{3+[M2]} \cdot O^{2-}] + 1/2\ H_2\uparrow$. Whereby the amount of Fe^{2+} at M1 seems to remain unchanged. This conclusion is supported by the experiments of Skogby and Rossman (1989) who found reversibly that in cpx heated in a hydrogen atmosphere H incorporation was correlated with increase of Fe^{2+} in the M2 site. But they argue against occupancy of the M2 position with Fe^{3+} because of the polydedron size and, they explained their observation by exchange of Fe^{2+} among M1 and M2 during the annealing. However, our crystal structure refinements of group A samples do not show such a fractionation of Fe^{2+} at M1 during annealing. As all samples annealed except Ur-1 originate from high temperature regimes (Table 1), they already reached high temperature equilibration. Thus, we suggest that in samples with relatively high Fe^{2+} concentration at M2 (around 0.1 pfu) and low water content (< 0.01) – it is the iron at M2 which oxidizes to Fe^{3+} for charge balancing the H loss through annealing. In such samples the probability to find a Fe^{2+M2} close to an OH group is higher than in samples with a low Fe^{2+} concentration at M2. The oxygen O2 which is involved in the OH bonds and which is in the case of dehydration undercharged belongs to both polyhedra, the M1 with a M1-O distance of 1.86 Å and to M2' with a M2'-O distance of 2.37 Å. Samples with

low concentration of Fe^{2+} at M2 (around 0.05 pfu) and relatively high water content (0.014) dehydrate through oxidation of Fe^{2+} at M1. Hercule and Ingrin (1999) observed for diopside which are relatively Fe-rich ($x_{Fe} > 0.08$) that the kinetic of the dehydration reaction $[Fe^{2+}\cdot OH^-] = [Fe^{3+}\cdot O^{2-}] + 1/2\ H_2\uparrow$ is fast and rate-limited by the mobility of the hydrogen atoms whereas, for lower iron contents the kinetic is slower and controlled by the mobility of electron holes. Maybe this explains our observations: in samples with x_{Fe} at M2 around 0.1 pfu dehydration is very fast and controlled by the mobility of hydrogen and oxidation of Fe^{2+} at M2 while in samples with x_{Fe} <0.05 dehydration is slower and controlled by the mobility of electron holes and oxidation of Fe^{2+} at M1.

It would be a great challenge to check the natural untreated samples with low water contents for the presence of Fe^{3+} at M2. The most promissing candidate which could have lost its water during uplift is sample DB22 which contains only 50 ppm H_2O by weight although it experienced high pressure and temperature. Unfortunately the low absorption intensity of its Mössbauer spectrum does not allow us to check for the presence of Fe^{3+} at M2 using our 4D fit model.

Conclusions

In this study we quantitatively describe the dehydration process of omphacite using our experimentally determined absorption coefficient for water in omphacite as $\varepsilon_{i,tot} = 65000 \pm 3000\ lmol_{H2O}^{-1}cm^{-2}$.

We simulated dehydration of omphacite during its uplift to the surface by annealing the samples in air. Dehydration of omphacite is a relatively fast process starting and ending at relatively low temperatures (from 550 °C to 780 °C). It is combined with an oxidation process according to $[Fe^{2+}\cdot OH^{-}]= [Fe^{3+}\cdot O^{2-}]+1/2\ H_2\uparrow$. Depending on the ratio of Fe^{2+M2}/H oxidation either occur at M2 (ratio >10) or at M1(ratio < 5). Thus, the presence of Fe^{3+} at M2 seems to be unique for dehydration events and might be an indicator for hydrogen loss during ascent. On the other side the absence of Fe^{3+} at M2 is not a proof against hydrogen loss. However, this assumption needs further proof.

Acknowledgment

We thank R. Schulz, O. Appelt and I. Schäpan for assistance in the different labs. Prof. G. Franz is thanked for providing some of the natual samples and Dr. M. Wiedenbeck for helpful discussions and suggestions concerning the SIMS measurements. The comments and suggestions of R. Stalder and an anonymous reviever helped to improve the manuscript.

References

Abs-Wurmbach I, Amthauer G (1988) Crystal chemistry of iron in natural and in synthetic braunites $Mn^{2+}(Mn^{3+}, Fe^{3+})_6O_8/SiO_4$. Z. Krist.1984:13 - 30

Bell DR, Ihinger PH, Rossman GR (1995) Quantitative analysis of trace OH in garnet and pyroxenes. Am Mineral 80: 465 - 474

Blanchard M, Ingrin J (2004) Hydrogen diffusion in Dora Maira pyrope. Phys Chem Minerals 31: 593 - 605

Burns RG (1993) Mineralogical applications of crystal field theory. Cambridge University Press, 2nd Edition, Cambridge

Carpenter MA (1983) Microstructures in sodic pyroxenes; implications and applications. In: Proceedings of the meeting on Application of mineral synthesis to high-pressure petrology; the real and average structures of synthetic and natural pyroxenes and amphiboles. pp. 271-301. Istituto di Mineralogia dell'Universita di Roma: Rome, Italy.

Dobretsov N.L., Sobolev NV., Schatskiy W.S. et al. (1989). Eclogite and glaucophane schist of fold mountains. Nauka, Novosibirsk, 236 p.

Dyar MD, McGuire AV, Ziegler RD (1989) Redox equilibria and crystal chemistry of coexisting minerals from spinel lherzolite mantle xenoliths. Am Mineral 74: 969 - 980.

Franz G, Thomas S, Smith DC (1986) High-pressure phengite decomposition in the Weissenstein eclogite, Münchberger Gneiss Massif, Germany. Contrib Mineral Petrol 92: 71 - 85.

Hammerschmidt K, Franz G (1992) Retrograde evolution of eclogites; evidences from microstructures and $^{40}Ar/^{39}Ar$ white mica dates, Muenchberg Massif, northern Bavaria. Contributions to Mineralogy and Petrology 111: 113 - 125

Hercule S, Ingrin J (1999) Hydrogen in diopside: Diffusion, kinetics of extraction-incorporation, and solubility. Am Mineral 84: 1577 - 1587

Ingrin J, Skogby H (2000) Hydrogen in nominally anhydrous upper-mantle minerals: concentration levels and implications. Eur J Mineral 12: 543 - 570

Katayama I., Nakashima S., Yurimoto H. (2006) Water content in natural eclogite and implication for water transport into the deep upper mantle. Lithos 86: 245 - 259

Koch-Müller M, Matsyuk SS, Rhede D, Wirth R, Khisina N (2006) Hydroxyl in mantle olivine xenocrysts from the Udachnaya kimberlite pipe. Phys Chem Minerals 33: 276 -287

Koch-Müller M, Matsyuk SS, Wirth R (2004) Hydroxyl in omphacites and omphacitic clinopyroxenes of upper mantle to lower crustal origin beneath the Siberian platform. Am Mineral 89: 921 - 931

Koch-Müller M., Abs-Wurmbach I., Bubenik W. (1999) Intracrystalline fractionation of Fe in synthetic (Fe, Mg, Zn) - bearing staurolite; a Mössbauer spectroscopic study. Phys Chem Minerals 26: 312 - 321

Langer K (1988) UV tio NIR spectra of silicate minerals obtained by microscope spectrometry and their use in mineral thermodynamics and kinetics. In Salje (ed.) Physical properties and thermodynamic behaviour of minerals. 639 - 685, D. Reidel Publishing Company

Li YL, Zheng YF, Fu B (2005) Mössbauer spectroscopy of omphacite and garnet pairs from eclogites; application to geothermobarometry. Am Mineral 90: 90 - 100

Libowitzky E, Rossman GR (1997) An IR absorption calibration for water in minerals. Am Mineral 82: 1111 - 1115

Maldener J, Hösch A, Langer K, Rauch F (2003) Hydrogen in some natural garnets studied by nuclear reaction analysis and vibrational spectroscopy. Phys Chem Minerals 30: 337 - 344

Nagel D (1990) The program “MBF”. Universität Marburg, Germany.

Oberti R, Caporuscio FA (1991) Crystal chemistry of clinopyroxenes from mantle eclogites: a study of the key role of the M2 site population by means of crystal- structure refinement. Am Mineral 76: 1141 - 1152

Paterson MS(1982) The determination of hydroxyl by infrared absorption in quartz, silicate glasses and similar materials. Bull Minéral 105: 20-29

Pouchou JL, Pichoir F (1985) "PAP" F(ρZ) procedure for imporved quantitative microanalysis. Microbeam Anal 1985: 104 - 106

Raheim A, Green DH (1974) Experimental determination of the temperature and pressure dependence of the Fe-Mg partition coefficient for coexisting garnet and clinopyroxene. Contrib Min Petrol 48: 179 - 203

Rhede D, Wiedenbeck M (2006) SIMS Quantification of Very Low H_2O Contents. Applied Surface Science 252: 7152 – 7154

Rossi G, Oberti R, Dal NA, Molin GM, Mellini M (1987) Residual electron density at the M2 site in C2/c clinopyroxenes; relationships with bulk chemistry and sub-solidus evolution. Phys Chem Minerals 14: 514 - 520

Sachs L. (1972) Statistische Auswertungmethoden. Springer Verlag, Berlin Heidelberg New York 3rd edition. Error progagation p. 78

Skogby H, Rossman GR (1989) OH in pyroxene: An experimental study of incorporation mechanisms and stability. Am Mineral 74:1059 –1069

Stalder R, Skogby H (2007) Dehydration mechanisms in synthetic Fe-bearing enstatite. Eur J Mineral 19: 201 - 216

Woods SC, Mackwell S, Dyar D (2000) Hydrogen in diopside: diffusion profiles. Am Mineral 85: 480 - 487

Wright SE, Foley JA, Hughes JM (2000) Optimization of site occupancies in minerals using quadratic programming. Am Mineral 85: 524 - 531

Yakovlev BG, Matsyuk SS, Wischnewskiy AA Tschubarov WM., Spetsius ZW (1990) The Evolution of mineral equilibria and petrogenesis of the deep mafic ferruginous granulites from Yakutian kimberlite piepes. Mineralogicheskiy Journal 12: N4: 3 - 15 (in Russian)

Figure Captions

Fig. 1: Some representative IR spectra of omphacite showing two groups of OH bands.

Fig. 2: Observed and resolved Mössbauer spectra of samples DB22 and Ur-1. RA%: Resonant absorption in %.

Fig. 3: Spectrum of sample Ur-1 taken from the UV-edge to the NIR.

Fig. 4: Spectra of samples Ur-1 and SA taken in the visible spectral range.

Fig. 5: (a.) NIR spectra of samle SA before and after annealing the sample under controlled reducing conditions (upper part) and before and after annealing the sample in air (lower part). (b.) Spectra in the visible of sample SA taken before and after annealing the samples at the specific temperature in air for 24 h.

Fig. 6: Infrared spectra of sample SA (a.) and sample Ur-1 (b.) taken before and after annealing the samples at the specific temperature in air for 24 h.

Fig. 7: Observed and resolved Mössbauer spectra of sample TW-2, before (a.) and after annealing (b., c.) using a three and four doublet model, respectively. RA%: Resonant absorption in %.

Fig. 8: Observed and resolved Mössbauer spectra of sample SA, before and after annealing (a., b. (3D), c.(4D)), sample Sl-415 before and after annealing (d. and e.), and sample Ur-1 after annealing (f.). RA%: Resonant absorption in %.

Fig. 9: NIR spectra of sample Sl-415 (a.) and spectra of sample Ur-1 in the visible and NIR (b. and c., respectively) taken before and after annealing the samples at the specific temperatures in air for 24 h.

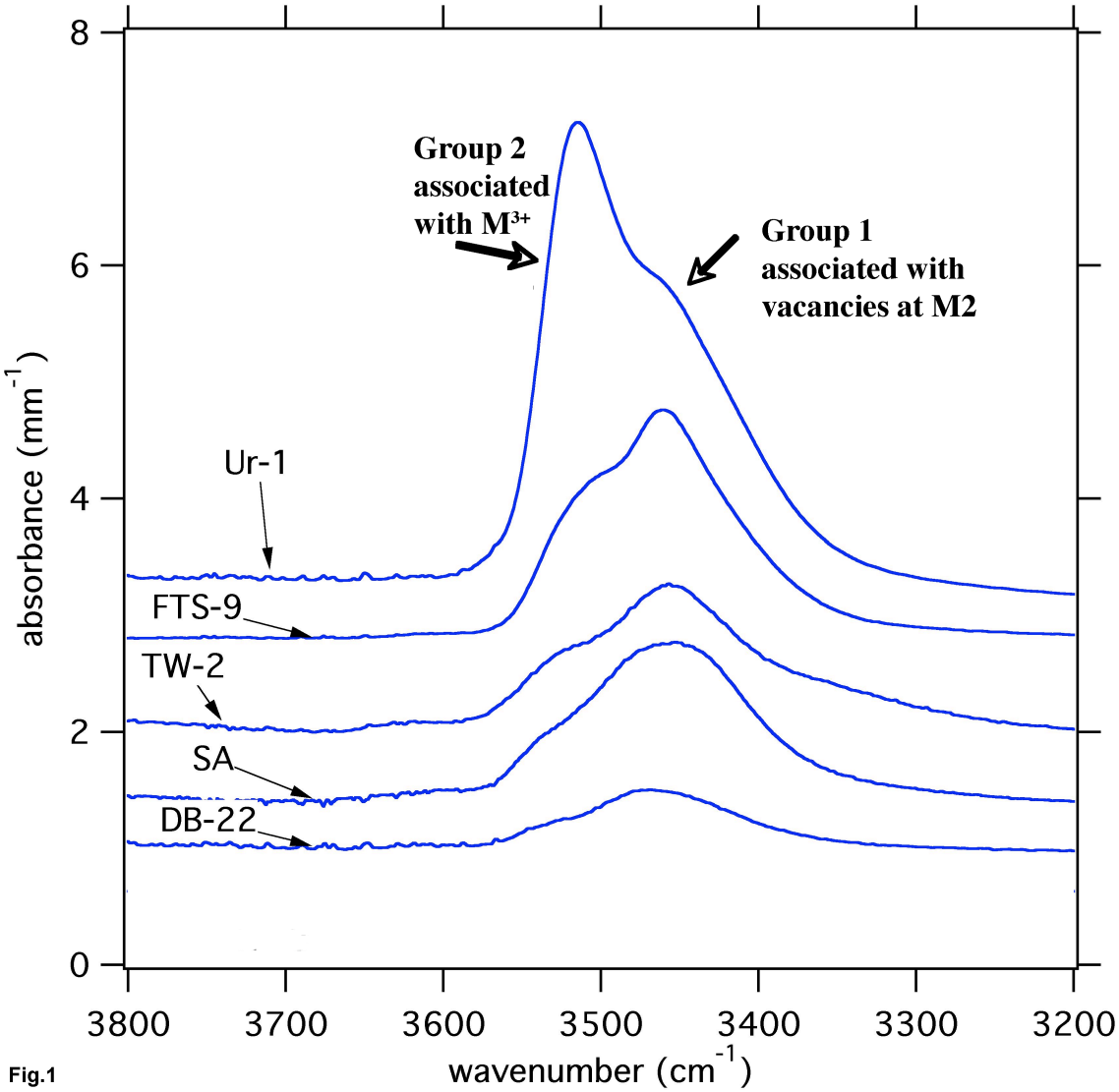
Group 2
associated
with M3+
Group 1
associated with
vacancies at M2
Ur-1
FTS-9
TW-2
SA
DB-22
absorbance (mm-1)
wavenumber (cm-1)
0
2
4
6
8
3800
3700
3600
3500
3400
3300
3200

Fig.1

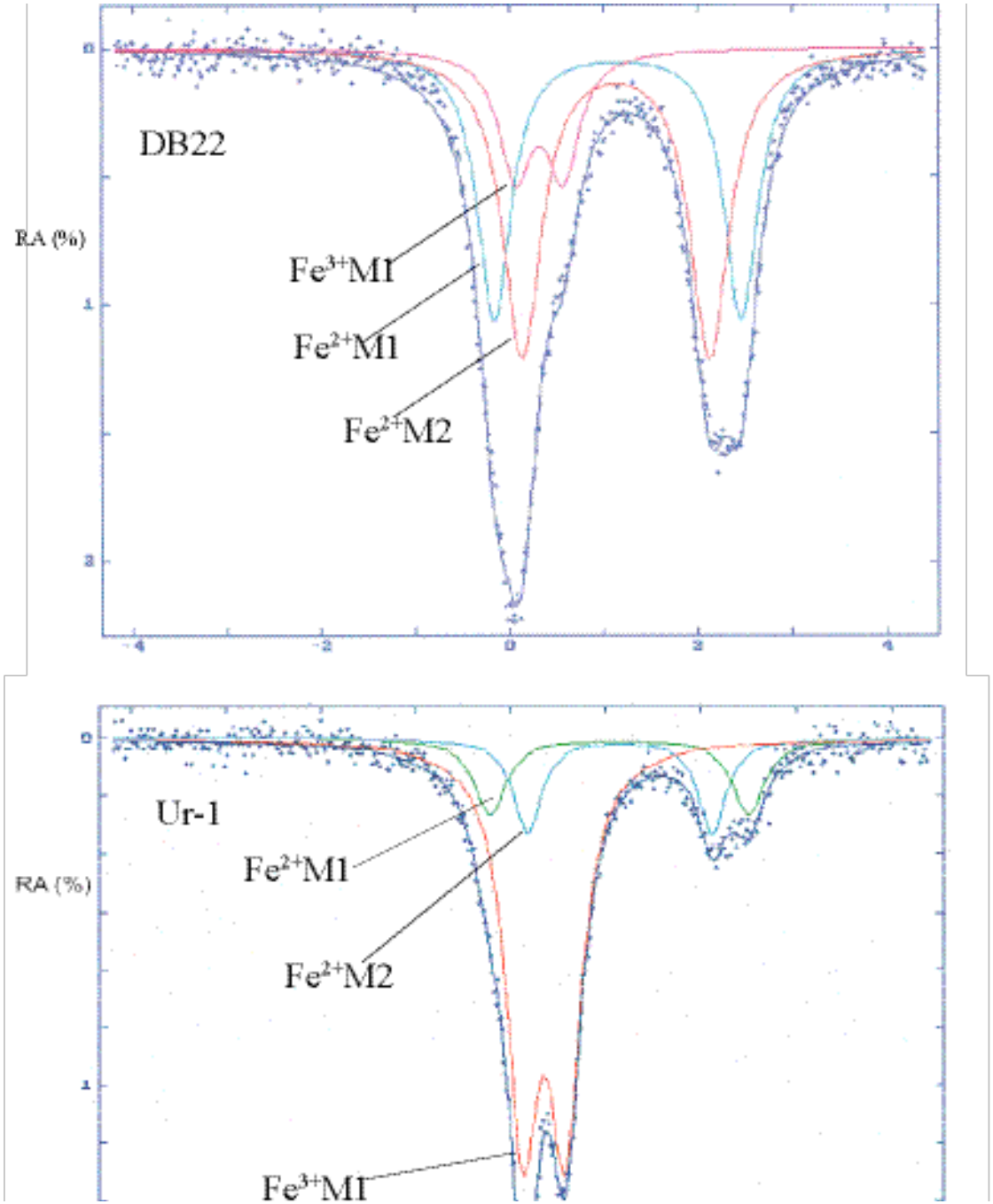
DB22
RA (%)
Fe3+M1
Fe2+M1
Fe2+M2
Ur-1
RA (%)
Fe2+M1
Fe2+M2
Fe3+M1

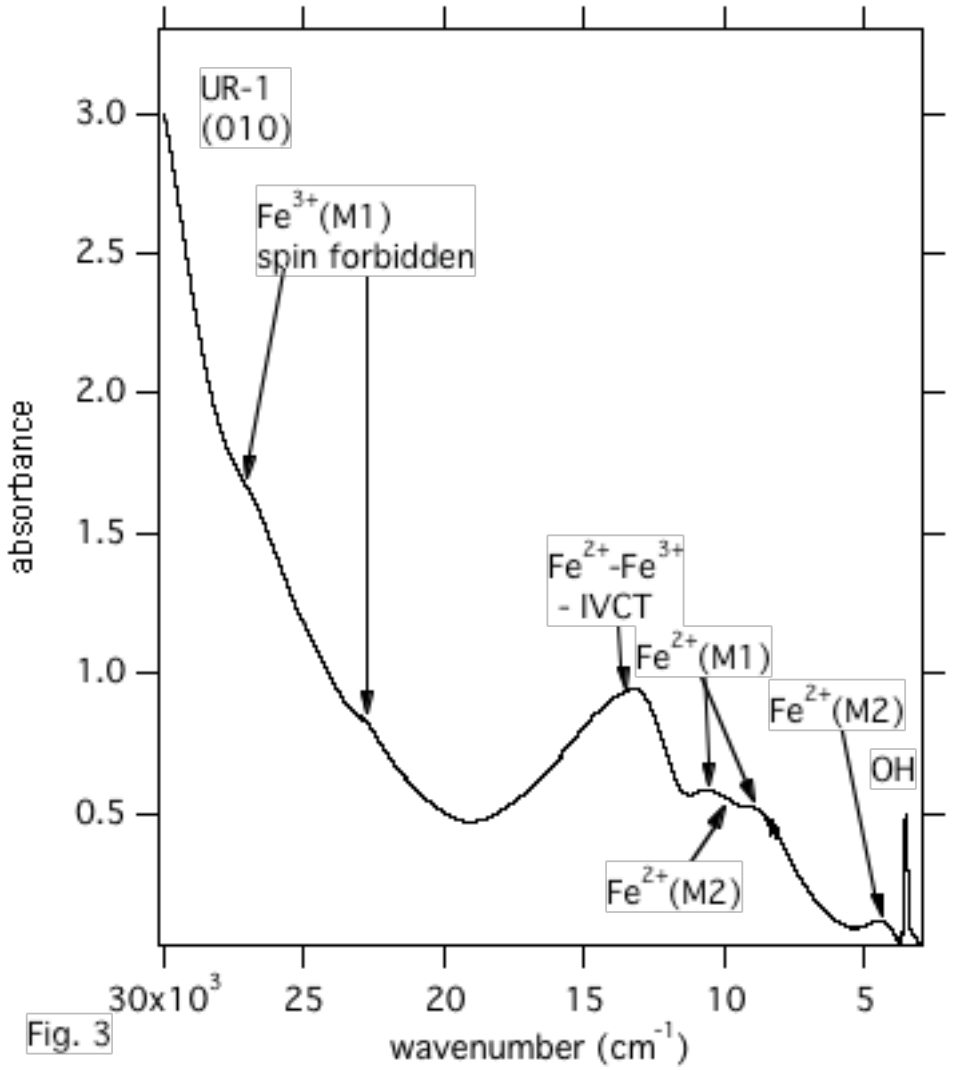
UR-1
(010)
Fe3+(M1)
spin forbidden
Fe2+-Fe3+
- IVCT
Fe2+(M1)
Fe2+(M2)
OH
Fe2+(M2)
absorbance
3.0
2.5
2.0
1.5
1.0
0.5
30x10^3
25
20
15
10
5
wavenumber (cm-1)

Fig. 3

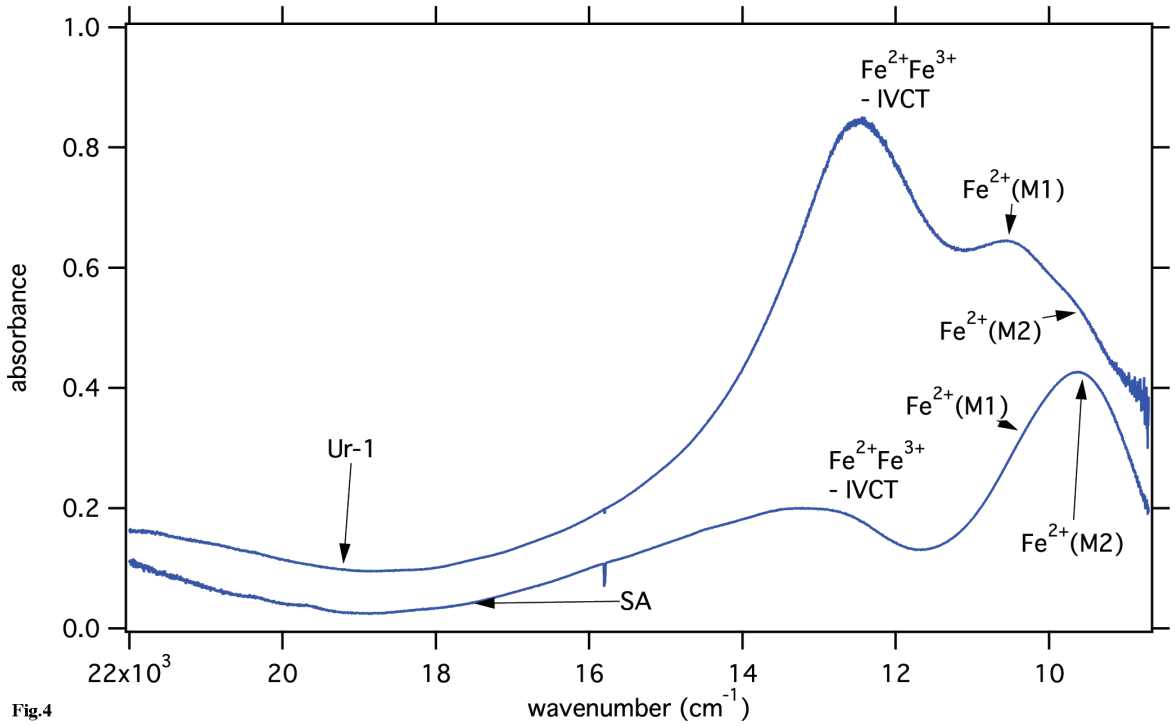
1.0
0.8
0.6
0.4
0.2
0.0
absorbance
22x10^3
20
18
16
14
12
10
wavenumber (cm^-1)
Fe2+Fe3+
- IVCT
Fe2+(M1)
Fe2+(M2)
Ur-1
SA
Fe2+(M1)
Fe2+Fe3+
- IVCT
Fe2+(M2)

Fig.4

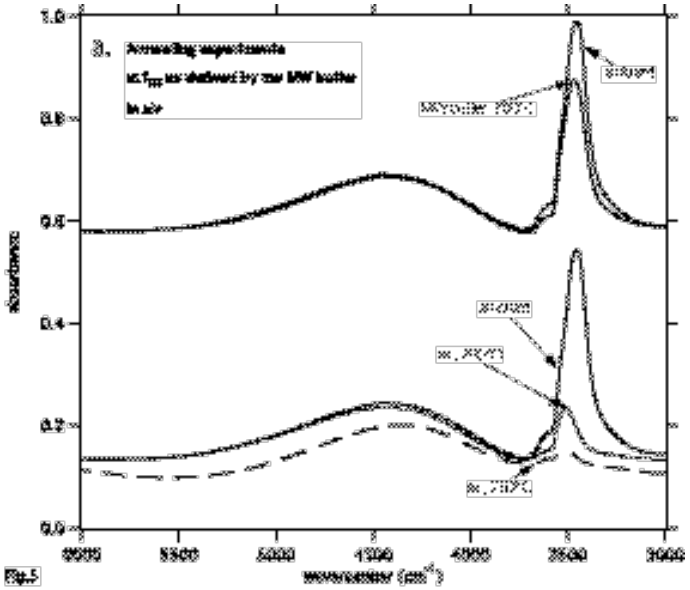

Fig.5

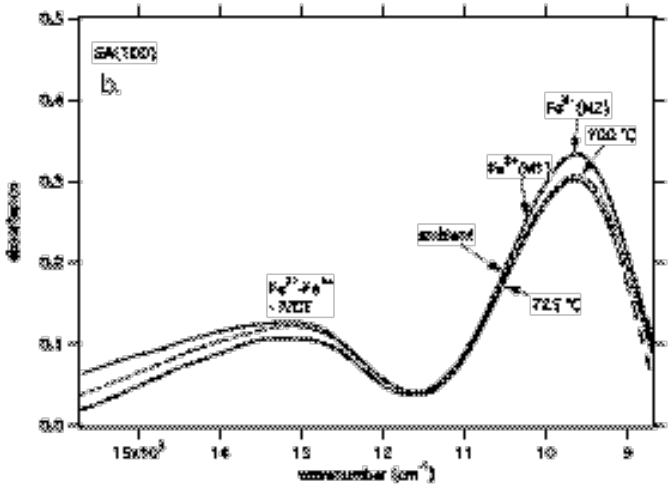

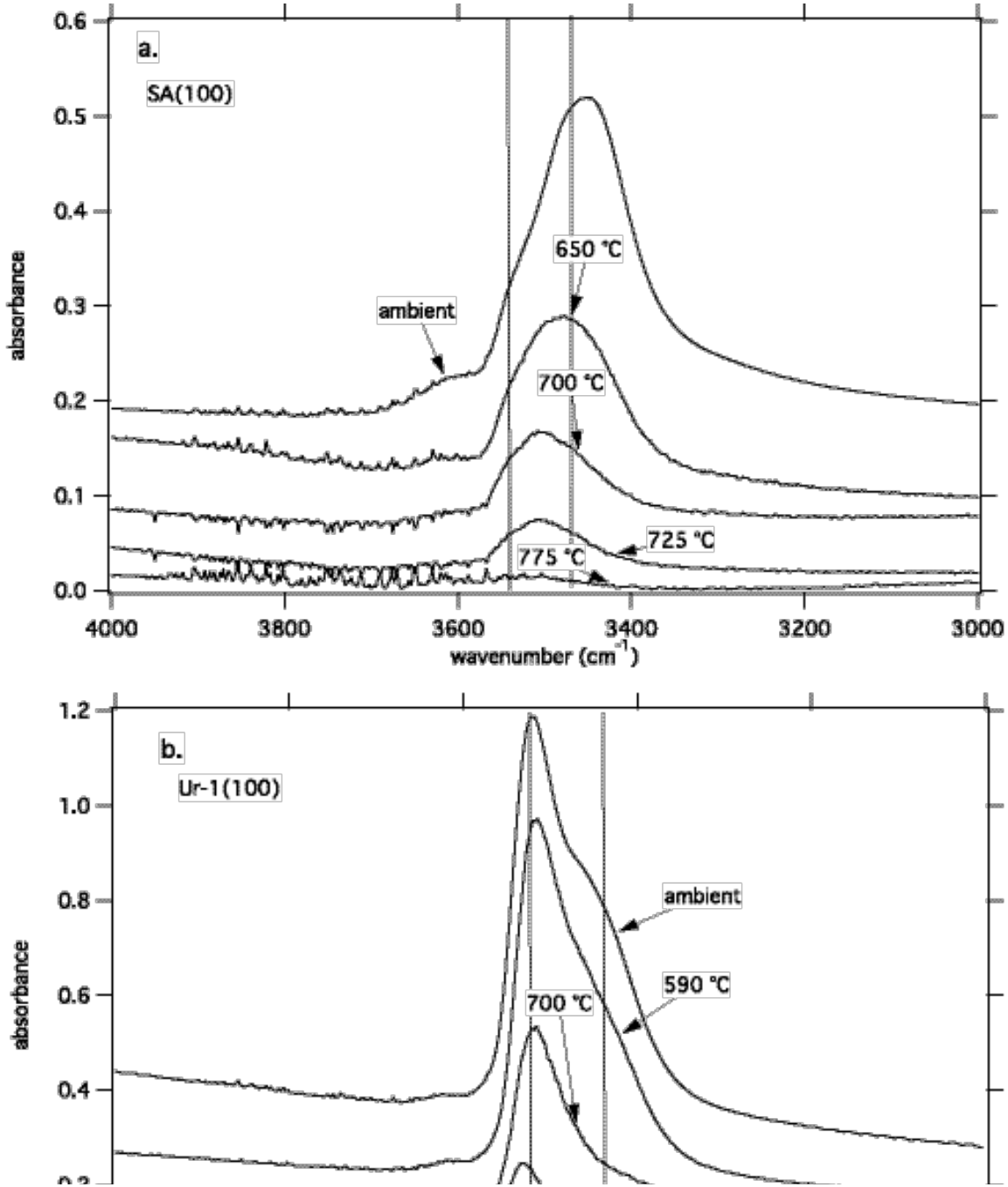
a.
SA(100)
ambient
650 °C
700 °C
725 °C
775 °C
absorbance
wavenumber (cm-1)
b.
Ur-1(100)
ambient
590 °C
700 °C
absorbance

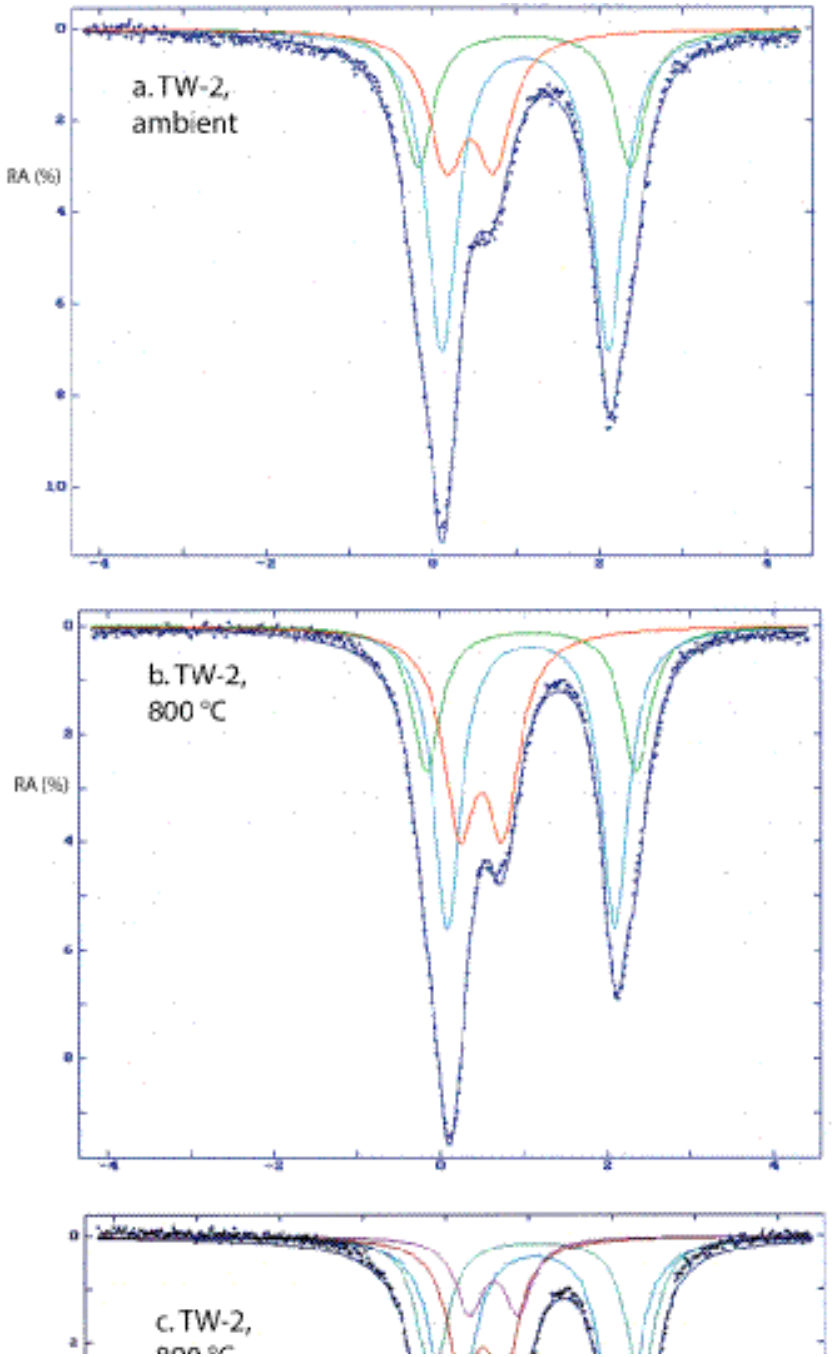
a. TW-2,
ambient
RA (%)
b. TW-2,
800 °C
RA (%)
c. TW-2,

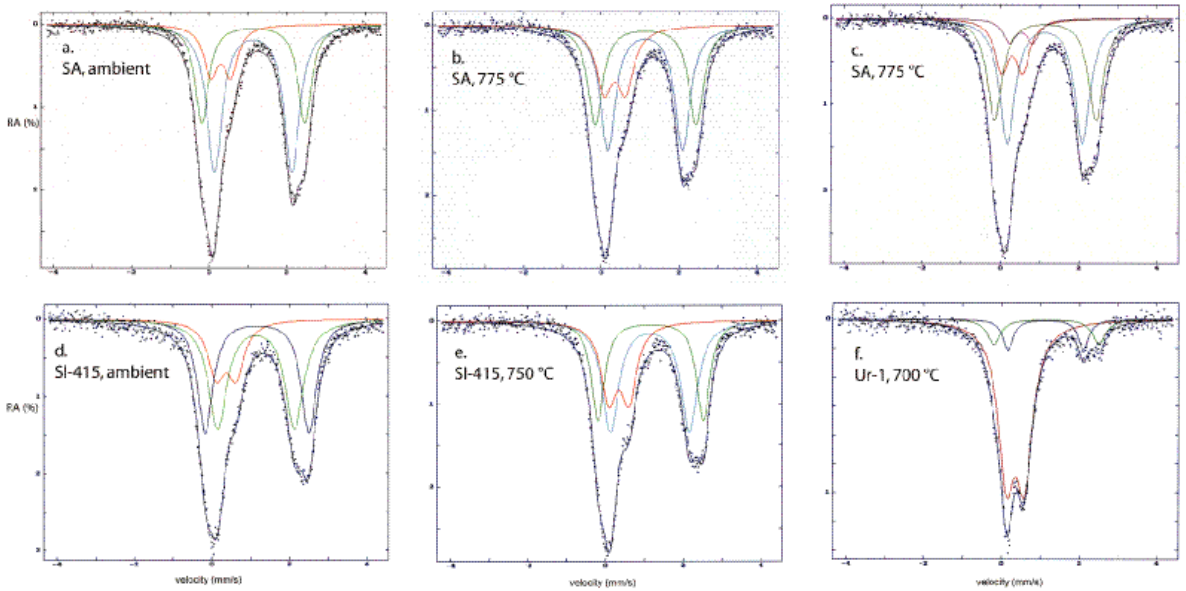
a.
SA, ambient
b.
SA, 775 °C
c.
SA, 775 °C
RA (%)
d.
Sl-415, ambient
e.
Sl-415, 750 °C
f.
Ur-1, 700 °C
RA (%)
velocity (mm/s)
velocity (mm/s)
velocity (mm/s)

Fig. 8

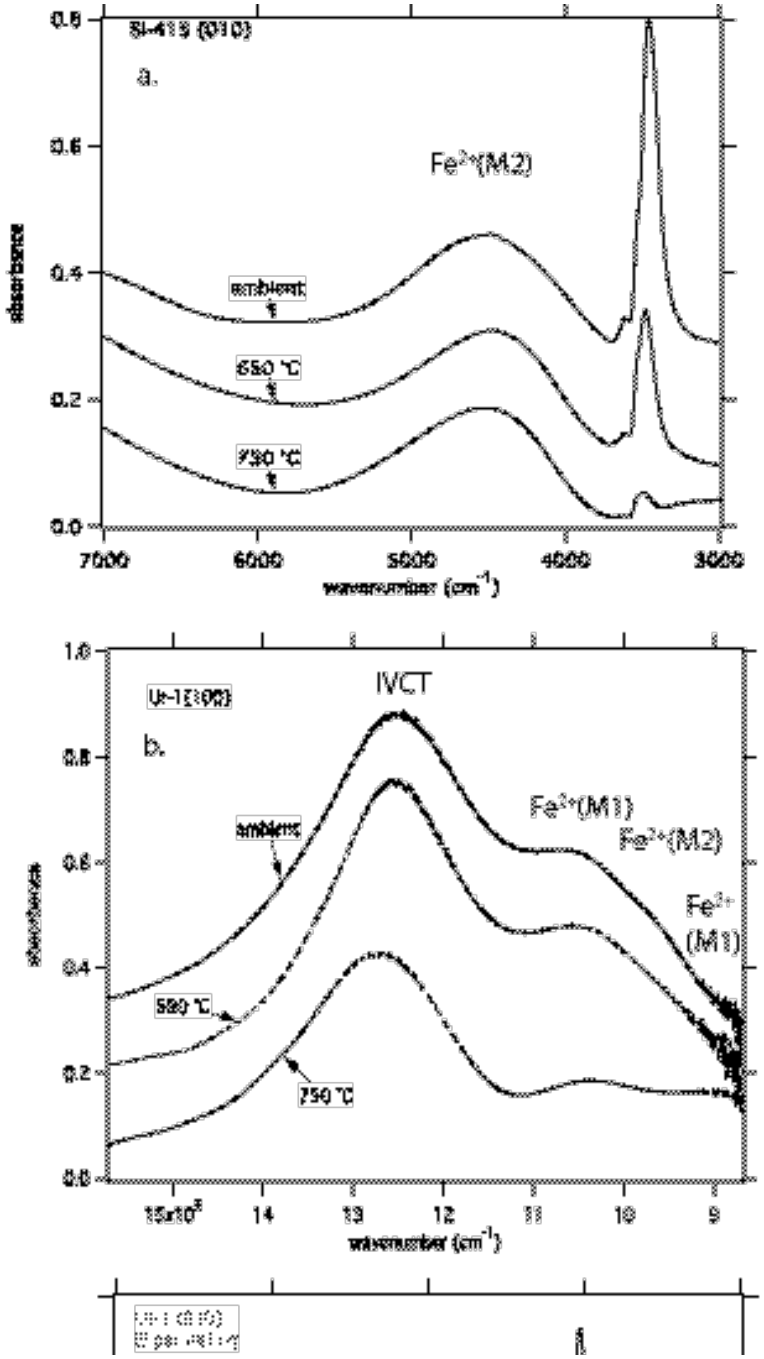
a.
Fe2+(M2)
ambient
650 °C
750 °C
absorbance
wavenumber (cm-1)
b.
IVCT
Fe2+(M1)
Fe2+(M2)
Fe2+
(M1)
ambient
500 °C
750 °C
absorbance
wavenumber (cm-1)

Table 1. Samples, localities, *P* and *T* estimates and water contents

Sample no	Locality	Rock	*Mineral composition* of the rock	*P*, GPa	*T*°C Space group	References	Ai,tot (mm^{-1})	wt ppm H_2O
DB-22†	De Beers pipe, South Afrika	Eclogite	$Gt_{45-50} + Cpx_{50-55}$	4.0-4.5	1120-1170 C 2/c		165	139
SA†	Kimberlites, South Afrika	Eclogite	$Gt_{40-45} + Cpx_{55-60} + Ru_{<1}$	3.0-3.7	810-860 C 2/c		451	378
Tw-297/77	Udachnaya pipe, Yakutia	Eclogite	$Gt_{40-42} + Cpx_{58-60}$	3.9-4.3	1050-1300 C 2/c	Koch-Müller et al. (2004)	61	51
Sl-415†	Slyudyanka pipe, Yakutia	Eclogite	$Gt_{43-45} + Cpx_{53-54} + Ru_1$	3.0-3.5	925-980 -		699	587
Tw-2	Udachnaya pipe, Yakutia	Mg-Fe-granulite	$Gt_{40} + Cpx_{20} + Amph_{10-15} +$ $+ Pl_{25} + Ilm_{2-3}$	1.6-2.0	900-1100 C 2/c	Yakovlev et al. (1990)	501	420
1131	Münchberger Massiv, Germany	Eclogite	$Gt_{50} + Cpx^{I}_{20-40} + Amph^{I}_{5} + Q_{5-10} +$ $+ Ru + Phn + (Cpx^{II}, Amph^{II}, Ep, Pl,$ Bi, Ap, Pmp, Sph, Zrk, K-Fld, Ca)	1,3-1,7	620±50 P 2/n	Franz et al. (1986)	698	586
FTS-9	Münchberger Massiv, Germany	Eclogite	$Gt_{20-25} + Cpx_{35-38} + Amph + Q +$ $+ Phn + (Pl, Bi, K\text{-}Fld, Pmp)$	1,3-1,7	620±50 P 2/n	Hammerschmidt & Franz (1992)	359	301
SB01-6	Münchberger Massiv, Germany	Eclogite	$Gt + Cpx + Amph + Q$	1,3-1,7	620±50 P 2/n	Hammerschmidt & Franz (1992)	496	416
Ur-1	Maksyutowskiy complex, South Ural, Russia	Eclogite	$Gt_{35-40} + Cpx_{15-20} + Amph_{20-25} +$ $+ Ru_{3-5} + Q_{10-15} + Ms_{<1} + Gl_{2-3}$	1.4-1.5	500-550 C 2/c	Dobretsov et al. (1989)	1031	865

*For abbreviations of mineral phases: Amph = amphibole, $Amph^{I,II}$ = amphibole I and II generations, Ap = apatite, Bi = biotite, Ca = calcite, Cpx = clinopyroxene, $Cpx^{I,II}$ = clinopyroxene I and II generations, Gl = glaukophane, Gt = garnet, Q = quarz, K-Fld = alkali feldspar, Ms = muskovite, Phn = phengite, Pl = plagioklase, Pmp = pumpellyite, Ru = rutile, Sph = Sphen, Zrk = zircon.
†*P*, *T*, calculated after Raheim and Green (1974).

Table 2: Chemical composition of the samples

	Tw-297	Sl-415	Tw-2	DB-22	SA	FTS-9	1131	SB01-6	Ur-1
MgO	10.70(8)	9.49(15)	11.25(7)	9.71(6)	11.04(7)	9.29(7)	9.35(52)	9.66(35)	7.78(15)
Na_2O	5.43(6)	5.53(20)	1.43(4)	4.68(7)	3.88(4)	6.21(5)	6.03(29)	5.74(23)	6.38(15)
Al_2O_3	8.62(15)	10.01(11)	3.34(30)	8.95(8)	8.16(8)	10.63(7)	9.67(99)	9.31(40)	8.25(18)
SiO_2	55.55(13)	54.74(29)	52.41(29)	53.92(20)	54.79(24)	56.27(14)	54.94(92)	55.15(36)	54.32(29)
CaO	15.53(12)	15.5(12)	20.08(15)	14.77(8)	16.73(13)	14.01(9)	15.10(42)	14.72(34)	13.29(15)
K_2O	0.06(1)	0.01(1)	0.01(1)	0.09(1)	0.05(1)	0.01(1)	0.00(1)	0.01(1)	0.00(1)
TiO_2	0.33(2)	0.26(3)	0.33(2)	0.83(2)	0.28(2)	0.11(2)	0.10(2)	0.09(3)	0.14(2)
MnO	0.04(2)	0.01(1)	0.08(2)	0.08(2)	0.04(3)	0.03(3)	0.02(2)	0.03(2)	0.03(1)
FeO	2.78(7)	3.64(7)	8.59(6)	6.14(6)	4.99(7)	3.47(9)	2.81(15)	3.11(7)	2.74(16)
Cr_2O_3	0.07(3)	0.06(3)	0.02(1)	0.03(2)	0.06(2)	0.05(2)	0.04(2)	0.04(1)	0.03(2)
Fe_2O_3	1.76(7)	0.95(7)	3.03(6)	1.28(6)	1.05(7)	0.96(9)	2.55(15)	3.03(7)	7.17(16)
H_2O	0.005	0.059	0.042	0.014	0.038	0.030	0.059	0.042	0.087
Σ	100.86	100.25	100.60	100.47	101.10	101.05	100.66	100.93	100.20
	normalized on the basis of 6 oxygens								
Mg	0.565	0.505	0.622	0.521	0.587	0.487	0.496	0.510	0.419
Al^{VI}	0.331	0.375	0.091	0.323	0.298	0.420	0.361	0.344	0.313
Fe^{2+}	0.027	0.050	0.080	0.080	0.055	0.036	0.032	0.026	0.040
Fe^{3+}	0.047	0.025	0.085	0.035	0.028	0.025	0.068	0.081	0.195
K	0.003	0.000	0.000	0.004	0.002	0.000	0.000	0.000	0.000
Ti	0.017	0.014	0.018	0.045	0.015	0.006	0.005	0.005	0.007
Mn	0.001	0.000	0.003	0.003	0.001	0.001	0.001	0.001	0.001
Cr	0.002	0.002	0.001	0.001	0.002	0.001	0.001	0.001	0.001
S M1	0.991	0.976	0.901	1.008	0.988	0.978	0.968	0.977	0.980
Na	0.373	0.383	0.103	0.327	0.268	0.424	0.416	0.395	0.446
Ca	0.590	0.593	0.798	0.570	0.640	0.528	0.576	0.559	0.514
Fe^{2+}	0.055	0.058	0.186	0.105	0.094	0.066	0.052	0.067	0.043
Σ M1+M2	2.005	2.010	1.988	2.010	1.990	2.000	2.012	2.000	1.983
Si	1.970	1.954	1.945	1.943	1.955	1.980	1.956	1.955	1.962

Al^{IV}	0.030	0.046	0.055	0.057	0.045	0.020	0.044	0.045	0.038
jd	0.326	0.358	0.018	0.292	0.240	0.398	0.348	0.315	0.252
ac	0.047	0.025	0.085	0.035	0.028	0.025	0.068	0.081	0.195
di	0.565	0.505	0.623	0.521	0.587	0.487	0.497	0.512	0.419
Ca-Tsch	0.029	0.044	0.054	0.057	0.044	0.019	0.042	0.039	0.035
he	0.027	0.050	0.080	0.080	0.055	0.036	0.032	0.026	0.040
$Fe^{2+\ M2}$/ $Fe^{2+\ M1+M2}$	0.671	0.568	0.619	0.647	0.647	0.631	0.699	0.518	0.537
H pfu	0.001	0.014	0.010	0.003	0.009	0.007	0.014	0.01	0.021
$H/10^6$ Si	604	6983	5201	1660	4501	3524	6950	4922	10425
$Fe^{2+\ M2}$/H	-	4.14	18.60	-	10.44	-	-	-	2.05

Σ = sum; jd = jadeite; ac = acmite; di = diopside; Ca-Tsch = Ca-Tschermakite;he = hedenbergite.

Tab. 3: Quantification and absorption coefficient of water in omphacite

	$A_{i,tot}$ (mm^{-1})	Wt ppm H_2O (SIMS)	$\varepsilon_{i,tot}$ ($lmol_{H2O}^{-1}cm^{-2}$)	Mean $\varepsilon_{i,tot}$ ($lmol_{H2O}^{-1}cm^{-2}$)
1131	698	568	67030	
SA	501	397	68834	65000 ± 3000
Sb1-6	446	402	60516	

Table 4: MS-parameters of natural omphacites.

Sample	TW297	DB22	1131	SB1-6	FTS9
χ^2	0.53	0.77	0.53	0.57	0.63
Exp/Calc	1.00	0.98	1.00	1.00	0.99
Fe^{2+} M1					
QS	2.66(2)	2.62(1)	2.78(1)	2.83(3)	2.81(1)
IS	1.13(1)	1.14(1)	1.14(1)	1.11(1)	1.16(1)
HW	0.41(2)	0.43(2)	0.44(2)	0.43 (4)	0.38(2)
T%	0.89(5)	1.05(4)	1.06(3)	0.27(2)	1.11(3)
Area	**21.0(8)**	**36.4(5)**	**24.5(5)**	**15.0(8)**	**28.0(6)**
(σ_f)%					
Fe^{2+} M2					
QS	2.05(2)	1.99(2)	2.02(3)	2.10(6)	2.06(1)
IS	1.10(1)	1.13(1)	1.12(1)	1.12(3)	1.16(1)
HW	0.52(2)	0.50(2)	0.45(2)	0.58(2)	0.46(1)
T%	1.43(5)	1.19(4)	1.32(3)	0.52(2)	1.69(3)
Area(σ_f)	**42.6(5)**	**47.7(4)**	**30.7(4)**	**38.2(4)**	**52.0(3)**
%					
Fe^{3+} M1 *(+M2)*					
QS	0.45(1)	0.51(2)	0.43(2)	0.48(4)	0.51(2)
IS	0.38(1)	0.32(1)	0.36(1)	0.34(2)	0.29(1)
HW	0.49(1)	0.42(2)	0.42(1)	0.55(1)	0.40(2)
T%	1.29(2)	0.47(2)	2.03(3)	0.67(1)	0.75(3)
Area	**36.4(3)**	**15.9(6)**	**45.5(2)**	**46.8(4)**	**20.0(6)**
(σ_f)%					

Isomer shifts (IS) are measured relative to IS of the metallic Fe°-foil used for calibration (c.f. chapter MS-Methods). This table summarizes those fits where all parameters were left free. Furthermore, fitting procedure was performed by direct fitting of doublets. Errors of IS, QS and of full half width HW at half height are rounded up to the 2nd digit (1s), even if the error in the third digit is less than 5. **Area (s_f):** areas and relative errors (**f** for fractional) are both given in %. Relative errors s_f of areas are rounded up/off to integers in %: e.g. 21.0(8) for TW297 means area 21.0% +/- 8%. In a first step Fe^{3+} is attributed to **M1**-position but, in case of

heating experiments in air, additionally **M2** occupation is expected (compare decrease and/or increase of Fe^{2+} in M1and M2).

Table 5: MS-Parameter of heat treated sample before and after heat treatment.

Sample	TW2	TW2 800 °C	TW2 800 °C	SA	SA 775 °C	SA 775 °C	SA 775 °C	Ur-1	Ur-1 700 °C	Ur-1 700 °C	SL-415	SL-415 650 °C	SL-415 750 °C
	free	free	2F	free	free	1F	1F	free	free	1F	free	free	free
$QSFe^{2+M1}$	2.58	2.52	2.52*	2.64	2.60	2.62	2.60*	2.71	2.71	2.71*	2.68	2.70	2.71
$ISFe^{2+M1}$	1.10	1.09	1.09*	1.13	1.14	1.13	1.14*	1.14	1.15	1.15*	1.16	1.16	1.17
$HWFe^{2+M1}$	0.41	0.41	0.41*	0.42	0.46	0.45	0.46*	0.41	0.41	0.41*	0.48	0.41	0.41
[Area (s_f)] %	20.5(6)	22.5(6)	23.5(1)	31.3(3)	33.7(3)	33.7(5)	34.5(1)	14.3(8)	10.9(2)	11.7(2)	37.6(6)	32.5(5)	30.4(6)
$QSFe^{2+M2}$	2.02	2.02	2.02*	1.99	1.92	1.90	1.92*	1.94	1.943	1.943*	1.99	2.06	2.04
$ISFe^{2+M2}$	1.10	1.09	1.09*	1.13	1.13	1.14	1.13*	1.15	1.134	1.134*	1.14	1.13	1.15
$HWFe^{2+M2}$	0.43	0.39	0.39*	0.48	0.48	0.48	0.48*	0.36	0.327	0.327*	0.58	0.49	0.52
[Area (σ_f)] %	56.2(2)	44.3(2)	43.9(1)	52.8(2)	43.2(2)	44.3(7)	43.3(1)	15.4(8)	10.6(14)	10.1(2)	43.4(6)	40.5(7)	42.7(5)
$QSFe^{3+M1}$	0.51	0.52	0.49(1)	0.51	0.55	0.46	0.54(1)	0.45	0.47	0.46(2)	0.51	0.45	0.52
$ISFe^{3+M1}$	0.50	0.49	0.44(1)	0.29	0.35	0.30 F	0.29(1)	0.35	0.36	0.36(1)	0.37	0.35	0.35
$HWFe^{3+M1}$	0.51	0.47	0.43(2)	0.44	0.52	0.40	0.43(3)	0.41	0.51	0.50(2)	0.53	0.50	0.49
[Area (σ_f)] %	23.4(3)	33.1(2)	21.2(8)	15.9(5)	23.2(4)	13.9(16)	15.5(9)	70.3(1)	78.5(2)	74.9(3)	19.1(6)	27.0(6)	26.9(6)
$QSFe^{3+M2}$			0.59(2)			0.78	0.59(2)			0.76(3)			
$ISFe^{3+M2}$			0.58(1)			0.41	0.52(2)			0.54(14)			
$HWFe^{3+M2}$			0.40 F			0.34	0.40F			0.40 F			
[Area (σ_f)] %			11.4(12)			8.2(24)	6.8(9)			3.3(6)			

Relative errors c.f. Tab. 4a. Procedere: in case of fixed HW values: errors were calculated by dividing error of T(Absorption) by the sum (HW+T): $\sigma_f = \sigma_f T/(HW+T)$). * fixed values taken from 3 D fit

Table 6: Details of single crystal X-ray diffraction

		DB22 (Before heat treatment)	DB22 (After heat treatment)
(A)	**Crystal data**		
	a (Å)	9.626(2)	9.620(2)
	b (Å)	8.803(2)	8.803(1)
	c (Å)	5.254(1)	5.254(1)
	β (deg)	106.85(1)	106.77(2)
	V ($Å^3$)	426.1(1)	426.0(1)
	Space group		*C* 2/*c*
	Z		4
	D_{calc} ($g\ cm^{-3}$)		3.406
	μ (mm^{-1})		2.428
(B)	**Intensity measurements**		
	No. of measured reflections	2031	2041
	No. of unique reflections	573	530
	R_{int} after absorption correction	0.039	0.045
	No. of observed reflections ($I > 2\ \sigma(I)$)	526	491
(C)	**Refinement**		
	No. of parameters used in the refinement	49	49
	R1 ($F_o > 4\ \sigma(F_o)$) ; R1 (all data)	0.025 ; 0.030	0.024 ; 0.039
	wR2 ($F_o > 4\ \sigma(F_o)$)	0.068	0.061
	Goodness of Fit	1.248	1.080

Final $\Delta\rho_{min}$ (e / Å^3)	-0.51	-0.35
Final $\Delta\rho_{max}$ (e / Å^3)	0.64	0.59

$R1 = \Sigma \, ||F_o| - |F_c|| \, / \, \Sigma \, |F_o|$ $\quad wR2 = (\Sigma(w(F_o^2 - F_c^2)^2) / \Sigma(w(F_o^2)^2))$

$w = 1 / (\sigma^2 (F_o^2) + (aP)^2)$ $\quad P = (2F_c^2 + \max(F_o^2, 0)) / 3$

Table 7: Heat-Treatment of the sample

Sample	T °C	H pfu (IR)	Fe^{3+} pfu (MS)	Fe^{2+} pfu (MS)
SA	775	0.000	0.041	0.136
	ambient	0.009	0.028	0.149
delta		-0.009	0.013	-0.013
SL-415	750	0.002	0.036	0.098
	ambient	0.013	0.026	0.109
delta		-0.011	0.010	-0.011
Ur-1	700	0.009	0.217	0.060
	ambient	0.021	0.195	0.083
delta		-0.012	0.022	-0.023
TW2	800	0.000	0.115	0.235
	ambient	0.010	0.085	0.266
delta		-0.010	0.030	-0.031